Frontiers of Information Technology & Electronic Engineering
www.jzus.zju.edu.cn; engineering.cae.cn; www.springerlink.com
ISSN 2095-9184 (print); ISSN 2095-9230 (online)
E-mail: jzus@zju.edu.cn

Adaptive compression method for underwater images based on perceived quality estimation*

Ya-qiong CAI, Hai-xia ZOU, Fei YUAN‡

Key Laboratory of Underwater Acoustic Communication and Marine Information Technology Ministry of Education, Xiamen University, Xiamen 361005, China

E-mail: caiyaqiong@stu.xmu.edu.cn; 850605461@qq.com; yuanfei@xmu.edu.cn

Received Nov. 9, 2017; Revision accepted Sept. 13, 2018; Crosschecked Mar. 27, 2019

Abstract: Underwater image compression is an important and essential part of an underwater image transmission system. An assessment and prediction method of effectively compressed image quality can assist the system in adjusting its compression ratio during the image compression process, thereby improving the efficiency of the image transmission system. This study first estimates the perceived quality of underwater image compression based on embedded coding compression and compressive sensing, then builds a model based on the mapping between image activity measurement (IAM) and bits per pixel and structural similarity (BPP-SSIM) curves, next obtains model parameters by linear fitting, and finally predicts the perceived quality of the image compression method based on IAM, compression ratio, and compression strategy. Experimental results show that the model can effectively fit the quality curve of underwater image compression. According to the rules of parameters in this model, the perceived quality of underwater compressed images can be estimated within a small error range. The presented method can effectively estimate the perceived quality of underwater compressed images, balance the relationship between the compression ratio and compression quality, reduce the pressure on the data cache, and thus improve the efficiency of the underwater image communication system.

Key words: Underwater image compression; Set partitioning in hierarchical trees; Compressive sensing; Compression quality estimation

https://doi.org/10.1631/FITEE.1700737 **CLC number:** TP391.41

1 Introduction

Images serve as eyes in underwater autonomous equipment and enable a visual effect that is expressed with difficulty through voice or text. They are therefore increasingly becoming the main carrier of underwater wireless communication as they are deployed to bear the broad and pressing demands for marine exploration, national security, and many other applications. The main difficulty in current underwater image applications is the contradiction between large volume of data in an underwater image and the acoustic communication bandwidth.

Given the combined conditions of limited channel bandwidth and certain communication transmission rates, image data need to be compressed as much as possible to improve the efficiency of image communication. However, to guarantee the quality of the reconstructed image, the transmitter needs to preserve as much image data as possible. An important part of image compression is the effective trade-off between the compression ratio and the compression quality. Kourzi et al. (2005) researched raising compression ratios while improving reliability by

‡ Corresponding author

* Project supported by the National Natural Science Foundation of China (Nos. 61571377, 61771412, and 68713367) and the Fundamental Research Funds for the Central Universities, China (No. 20720180068)

ORCID: Fei YUAN, https://orcid.org/0000-0002-8614-8756

analyzing the impact of filter group parameters on the compressed image, and the analysis results determined the selection of the filter in the process of encoding. A linear regression estimation model of different filters and compression qualities was established by Sarita et al. (2011), using a predictive model to assess the compression effect of the filter before image coding. Sophia and Anitha (2016) discussed the relationship between different region-of-interest (ROI) sizes and the compressed image quality, and then built a quality estimation model to predict the compression image quality from ROI and to choose a proper compression algorithm. The image quality estimation model was then used for image classification to demonstrate improved performance through the setting of different compression parameters for different images types (Tichonov et al., 2016).

However, in the above research only the compression part was considered, and there was less comprehensive research into combining image characteristics and channel conditions. In underwater communication, storage space and bandwidth allocation, as well as algorithm complexity, all need to be considered. To that end, a fast estimation model for compressed image quality based on perception mapping and an underwater image adaptive compression method is proposed in this study. First, IAM is used to distinguish the different image characteristics. Then, based on a summation of rules of different image compression methods, a perceived service quality vector is used to deconstruct the complexity of the IAM-BPP-SSIM relationships into several two-dimensional (2D) relationships. Finally, an estimation formula is obtained, so that the image compression quality can be estimated quickly using the image's IAM value. The quality of the compressed images can thus meet the needs of human eyesight using this estimation formula. In addition, the storage space can be used better and the bandwidth source can be allocated better.

2 Underwater image features and compression methods

Given limited energy of underwater nodes and bandwidth, to meet the needs of compressing images, a certain degree of compression distortion is allowed by current compression strategies for underwater images because of ineffective visual perception. The difficult part in underwater image communication is how to set the compression ratio accurately in accordance with visual perception (Tang et al., 2017). Any compression rate setting is related to not only the encoder, but also the communication link; thus, it needs to take the features of the link into consideration, and then the reference compression ratio can be obtained. The image is compressed by sparse transform in traditional methods. The energy is concentrated in a few coefficients, which are set below a certain threshold to realize the compression. The peak signal-to-noise ratio (PSNR) method is mainly used to measure the distortion effect after compression. However, there is a deviation between PSNR and human visual perception; thus, traditional methods can only rely on experiences to set the threshold, and cannot be optimally adjusted according to actual situations. Therefore, it is difficult to accurately find the inflection point using the energy method. In the compression of underwater images, as far as the performance effect of the codec is concerned, the coding error effect of the channel bit error rate needs to be considered. The resulting deficiency in an underwater acoustic channel thus greatly challenges quality control when the underwater images have a large amount of data, because images usually need to be compressed and adapt to an extremely limited bandwidth. Because of the time-variance of a multipath underwater acoustic channel, a single compression scheme has difficulty in adapting to such swiftly changing channel conditions.

Different compression encoding schemes for different channel characteristics are established in this study, and the perceived quality is used as the optimization criterion of image compression. An adaptive compression mechanism for underwater images under different channel conditions is proposed. The principle block diagram is shown in Fig. 1. First, different compression ratios are set for images with different IAMs under different compression methods. The quality of the reconstructed image is evaluated and the rules of the compression image quality are summarized. Subsequently, the perceived qualities of different images using different compression methods are modeled, and the IAM is mapped according to the compression rate and quality. Then a fast estimation system is generated. Finally, an image compression coding strategy is obtained according to IAM and channel conditions. The compressed image

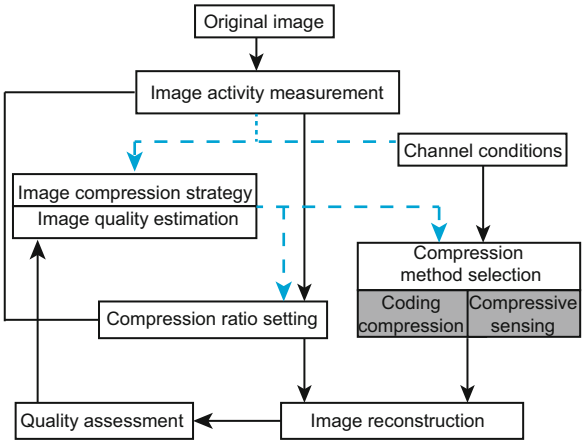

Fig. 1 Mechanism of underwater image adaptive compression

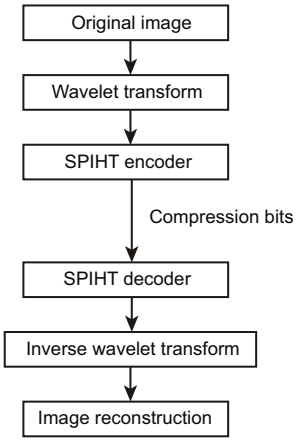

Fig. 2 The principle of set partitioning in hierarchical trees (SPIHT) compression algorithm

code stream is suitable for the transmission channel, and the image reconstruction quality conforms to the requirements of visual perception.

2.1 Image compression strategy based on encoding compression

An image's energy is reassigned after wavelet transform is performed, because the wavelet coefficients in different frequencies represent different information from the image. For example, low frequency coefficients contain the most information about an image, while high frequency coefficients reflect the edges and texture of an image. Wavelet transform cannot directly compress an image, but wavelet coefficients do enable good conditions for efficient image compression. Embedded coding is the most widely used algorithm because it makes the most of wavelet transform. Embedded coding encodes the important wavelet coefficients according to the compression ratio, which can accurately control the code flow. Underwater images were compressed using embedded zerotree wavelets encoding (EZW), adaptively scanned wavelet difference reduction (ASWDR), spatial-orientation tree wavelet (STW), and set partitioning in hierarchical trees (SPIHT) algorithms in Atallah et al. (2016). The experimental results showed that SPIHT achieved the best image reconstruction quality under the same compression ratio, and SPIHT is used in this study.

SPIHT (Said and Pearlman, 1996) compression algorithm's principle is shown in Fig. 2. First, the image is subjected to wavelet transform, and deconstructed into subbands of different frequencies. On the basis of different subband coefficients making different contributions to the image reconstruction, the important coefficients are priority encoded and control the length of each compressed bit stream according to the compression ratio.

The SPIHT compression algorithm is based on the combination of image wavelet coefficients and human visual characteristics. If the quality of a reconstructed image under a low compression ratio is good, then SPIHT has a simple structure and low complexity. SPIHT encodes the important information of an image based on priority, so the information contributing the most to image reconstruction is sent at the front of the bit stream. However, these important bits are more sensitive to errors, so often one bit error can make the reconstructed image difficult to recognize. Data bits in different positions have different importance, so when an important bit has an error, there is a greater impact on image reconstruction quality. The reconstructed image can appear with color piece accumulation and pixels disarranged, or lack the ability to produce appropriate image information from the original image. Therefore, the robustness of SPIHT code flow is poor, and the important bits in the code flow need to be protected during transmission.

2.2 Image compression strategy based on compressive sensing

Compressive sensing (CS) theory was proposed in Candès et al. (2006) and Donoho (2006). Compressive sensing theory consists primarily of sparse signal representation, random coding measurement,

and signal reconstruction. Initially, CS combines the signal's sampling and compression, and completes its compression once the signal is sampled at a lower rate. A discrete real value signal, $\boldsymbol{x}$ of length N, can be expressed as a basis linear set:

$$\boldsymbol{x} = \boldsymbol{\Psi a}. \tag{1}$$

When the projection of signal $\boldsymbol{x}$ on a basis $\boldsymbol{\Psi}$ has only K ($K \ll N$) non-zero coefficients, $\boldsymbol{x}$ can be regarded as a sparse signal on the basis of $\boldsymbol{\Psi}$. The encoding measurement model in compressive sensing theory does not directly measure signal $\boldsymbol{x}$, but projects to the set of low dimensional measurement vectors $\boldsymbol{\Phi}$ by uncorrelated measurement; the measured values are obtained as

$$\boldsymbol{y} = \boldsymbol{\Phi x} = \boldsymbol{\Phi\Psi a} = \boldsymbol{\Theta a}. \tag{2}$$

Because the number of the measured values $\boldsymbol{y}$ is far smaller than the number of the sparse coefficients $\boldsymbol{a}$, the compression sampling of the signal has been realized. To guarantee the convergence of the algorithm, sparse coefficients $\boldsymbol{a}$ can be restored accurately by the measurement values $\boldsymbol{y}$, where the measurement matrix must satisfy the restricted isometric properties (RIP) criterion. For any sparse vector $\boldsymbol{v}$, matrix $\boldsymbol{\Theta} = \boldsymbol{\Phi\Psi}$ can ensure that the following type is true:

$$1 - \varepsilon \le \frac{\|\boldsymbol{\Theta v}\|_2}{\|\boldsymbol{v}\|_2} \le 1 + \varepsilon, \tag{3}$$

where $\varepsilon > 0$. When the convergence of the algorithm is guaranteed, the reconstruction signal can be realized by solving the optimization problem of the norm.

CS has a good anti-noise performance because the reconstruction algorithm can obtain the important K sparsity component and suppress the other noise components to zero. Because the RIP rules have a limiting function, all of the measured values for the reconstruction algorithm have the same importance; in other words, there is no difference in the measured values of an image, so CS in communication and channel coding has high quality robustness.

Image blocks are sampled and measured according to the bispectrum and IAM (Chen et al., 2016). Image blocks with different saliency are assigned different sampling rates, since experiments show that this method has better image compression quality and higher robustness. The frame process for adaptive compression of underwater images is shown in Fig. 3.

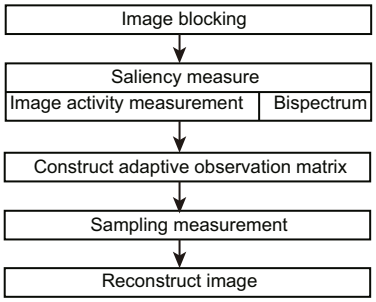

Fig. 3 Adaptive compression sensing flowchart

3 Mapping between image activity measurement and compression quality

3.1 Image activity measurement

Images with different texture complexity also have different degrees of redundancy, and the qualities of reconstructed images in the same compression ratio are different. Images with a simple structure and fewer textured edges have less information and a larger degree of redundancy; therefore, the reconstruction quality of images with a simple structure will be better than the reconstruction quality of images with a complex texture structure when compressed at a low compression ratio. It follows that images with a complex structure and more textured edges have a larger amount of information and lower redundancy. At the same compression rate, the complex image has lost more information after compression, so its reconstruction quality will be inferior to that with a simple structure. Therefore, on the premise that the perceived quality of a compressed image is not affected, image compression needs to set different optimal compression ratios for images with different texture complexities.

Image activity measure (IAM) can be regarded as an indicator of the complexity of the image (Saha and Vemuri, 2002). Using the same compression ratio, the higher the IAM of the image is, the poorer the image compression quality will be. The image region with edge and texture is defined as the "image active area"—the more complex the active areas are, the higher the IAM of the image will be. The saliency of the image is set based on IAM:

$$\begin{aligned}\mathrm{IAM}_0 = &\frac{1}{MN}\left[\sum_{i=1}^{M-1}\sum_{j=1}^{N}\sqrt{\boldsymbol{I}(i,j)-\boldsymbol{I}(i+1,j)}\right.\\ &\left.+\sum_{i=1}^{M}\sum_{j=1}^{N-1}\sqrt{\boldsymbol{I}(i,j)-\boldsymbol{I}(i,j+1)}\right],\end{aligned} \tag{4}$$

where M and N are the sizes of the image, $\boldsymbol{I}(i,j)$ means the the pixel value of the image at the point (i,j). The larger the value of the IAM is, the more complex the image structure will be. A smaller value indicates that the image structure is simpler and has less edge texture.

3.2 Compression image quality assessment

Image compression is accompanied by some loss of image information, though the degree of distortion of a compressed image is different under different compression ratios. The sensitivity of the human visual system differs according to the different structures and different frequencies of an image. Because the quality of visual perception is not proportional to the bit error rate, image quality cannot be measured depending only on the single bit error rate or the amount of information data. Therefore, it is necessary to choose one image quality evaluation index to effectively measure the quality of a compressed image, and then to evaluate image compression quality according to human visual characteristics.

Different quality evaluation algorithms have different sensitivity and accuracy in relation to the different types of images. The main aspects of distortion in image compression are fuzziness and blockishness caused by the quantization process; hence, we need to select the most effective evaluation algorithm for image compression.

Twenty clear underwater images were selected as reference images for building an underwater image database. The reference images were compressed using different compression rates (Table 1). The differences in image degradation are sometimes not obvious when the compression rate intervals are adjacent, so not all compressed images were selected. In the end, an underwater image database containing 200 images was built, where 15 respondents gave a mark 1–5 to each image. Then the image mean opinion score (MOS) was computed using the 15 subjective quality scores. The distribution of MOS is shown in Fig. 4, which demonstrates that the distorted images were perceived as covering various degrees of distortion.

Ten full reference image quality assessment algorithms (FRIQAs) were used to calculate the quality scores in the underwater image database. The performance of each FRIQA denotes the correlation of the objective score to MOS. We chose to use the Pearson correlation coefficient (PCC), the Spearman rank correlation coefficient (SRCC), the Kendall rank correlation coefficient (KRCC), and the root mean square error (RMSE) as our performance indices for each image quality assessment algorithm.

Table 1 Compression parameter settings of the underwater image database

Compression type	Compression rate	Number of selected images
SPIHT	0.05, 0.10, 0.15, 0.20, 0.3, 0.4, 0.5	5
CS	0.10, 0.15, 0.20, 0.25, 0.3, 0.4, 0.5	4

SPIHT: set partitioning in hierarchical trees; CS: compressive sensing

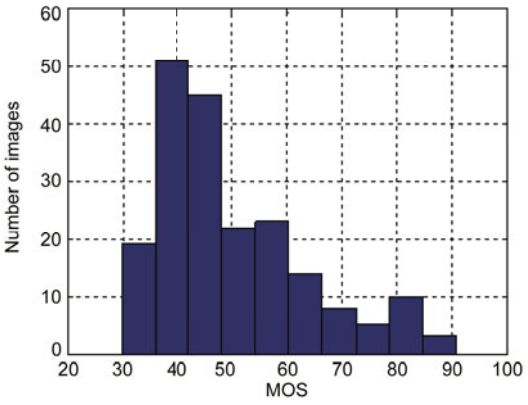

Fig. 4 Distribution of the mean opinion score (MOS) in the underwater image database

It can be seen from Table 2 that structural similarity (SSIM), feature similarity (FSIM), visual information fidelity (VIF), multi-scale SSIM (MS-SSIM), and gradient magnitude similarity deviation (GMSD) performed relatively well. SSIM is relatively simple, so it can be used as the quality perception index for the compressed image. SSIM combines the luminance, contrast, and structure of the original reference image and the distorted image to obtain its quality evaluation score, which corresponds to the main distorted features of the compressed image. SSIM is defined as

$$\mathrm{SSIM}(x,y)=\frac{(2\mu_x\mu_y+C_1)(2\sigma_{xy}+C_2)}{(\mu_x^2+\mu_y^2+C_1)(\sigma_x^2+\sigma_y^2+C_2)}, \quad (5)$$

where μ_x and μ_y are the average brightness values of a local pixel block of the original and distorted image respectively, σ_x and σ_y are the standard deviations of brightness of a local pixel in the two images, σ_{xy} is the correlation coefficient of brightness in the two corresponding pixels of the two images, and C is a small value.

Table 2 FRIQA performance in the underwater image database

Algorithm	SRCC	KRCC	PCC	RMSE
SSIM (Wang et al., 2004)	0.87	0.69	0.83	0.08
FSIM (Zhang et al., 2011)	0.89	0.72	0.83	0.04
FSIMc (Zhang et al., 2011)	0.89	0.71	0.83	0.04
GSM (Liu et al., 2012)	0.84	0.65	0.77	0.01
PSNR-HVS-M (Ponomarenko et al., 2007)	0.81	0.61	0.91	4.77
PSNR-HVS (Ponomarenko et al., 2007)	0.80	0.60	0.91	4.64
VIF (Sheikh and Bovik, 2006)	0.88	0.70	0.89	0.09
MS-SSIM (Wang et al., 2003)	0.88	0.70	0.67	0.07
UIQ (Wang and Bovik, 2002)	0.66	0.48	0.36	0.02
GMSD (Xue et al., 2014)	0.88	0.71	0.89	0.03

FRIQA: full reference image quality assessment; SRCC: Spearman correlation coefficient; KRCC: Kendall rank proliferation correlation coefficient; PCC: Pearson correlation coefficient; RMSE: root mean square error; SSIM: structural similarity; FSIM: feature similarity; FSIMc: a simple extension of FSIM; GSM: gradient similarity; PSNR-HVS: peak signal-to-noise ratio with human visual system; PSNR-HVS-M: modified PSNR-HVS; VIF: visual information fidelity; MS-SSIM: multi-scale SSIM; UIQ: universal image quality; GMSD: gradient magnitude similarity deviation

SPIHT compression and adaptive CS compression of the underwater images were performed, respectively. The compressed image and SSIM values of different compression rates are shown in Fig. 5.

Under a different compression ratio, the image distortion degree is also different. With the increase of BPP, image quality gradually increases, but the increasing trend is nonlinear. Because each compression method is different, the curve shape of BPP-SSIM is different. However, SSIM values of the images can better reflect the quality of image compression. The main distortion feature in SPIHT compression is fuzziness, where edges and textures broaden. The main distortion feature in adaptive CS compression is the lack of textual clarity, where a light colored area appears as a bright spot, where the foreground and background of the images are blended under a low compression ratio.

3.3 Mapping image activity measurement with perceived quality

For different kinds of images with different IAMs, the compression quality will differ by the same compression rate, and the corresponding compression quality curve will shift. To validate this compression phenomenon, six underwater images with different IAM_0 values were separately selected to perform SPIHT compression and adaptive CS compression. These images contained a single objective and multiple objectives, close shots and long shots, and simple texture/complex texture features (Fig. 6). In the low compression ratio (BPP=0.05–0.3), the compression step was set at 0.05, where the compression step is 0.1 at the higher compression ratio (BPP=0.3–0.9), so the range of the independent variable is 0.05–0.9. The SSIM value was set as the representation of image quality, where SSIM values of different images were calculated at different compression rates, with a plot drawn-scatter graph for each image. The results are shown in Fig. 7.

As shown in Fig. 7, the compression curves for different IAM_0 images are not precisely the same, but the trend for a set of curves follows the same basic

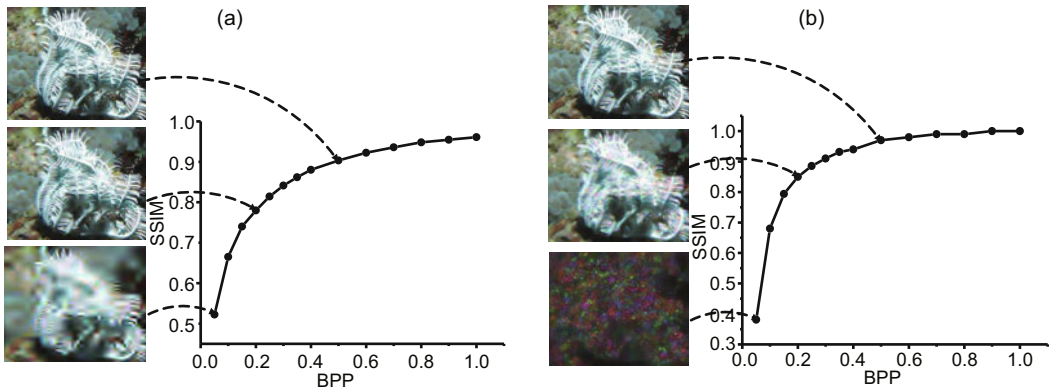

Fig. 5 Underwater image compression curve and effect: (a) SPIHT compression; (b) adaptive CS compression

SSIM: structural similarity; BPP: compression rate; SPIHT: set partitioning in hierarchical trees; CS: compressive sensing

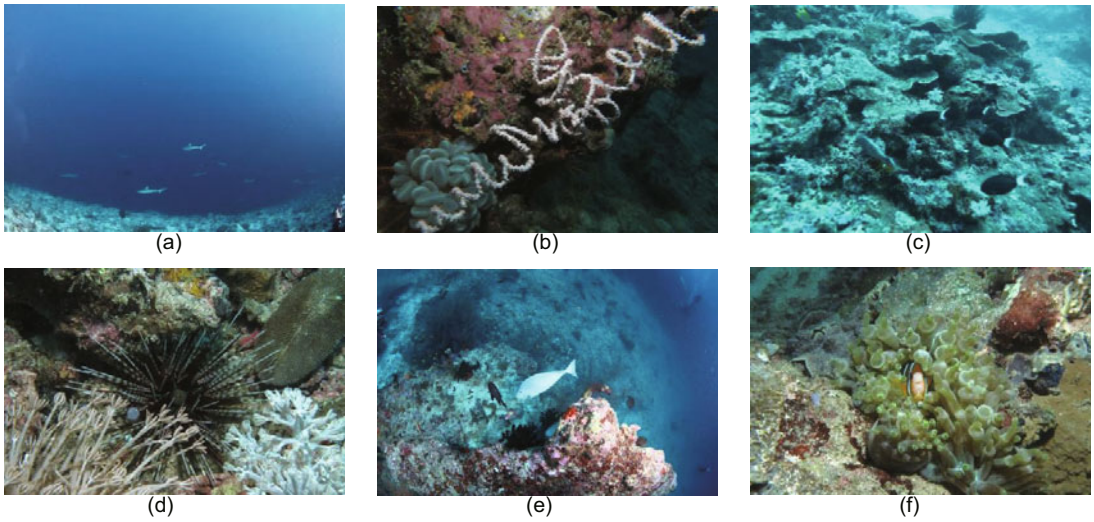

Fig. 6 Underwater images: (a) IMG20: IAM_0=7.3; (b) IMG9: IAM_0=16.8; (c) IMG19: IAM_0=25.8; (d) IMG6: IAM_0=35.7; (e) IMG7: IAM_0=45.2; (f) IMG3: IAM_0=50.1

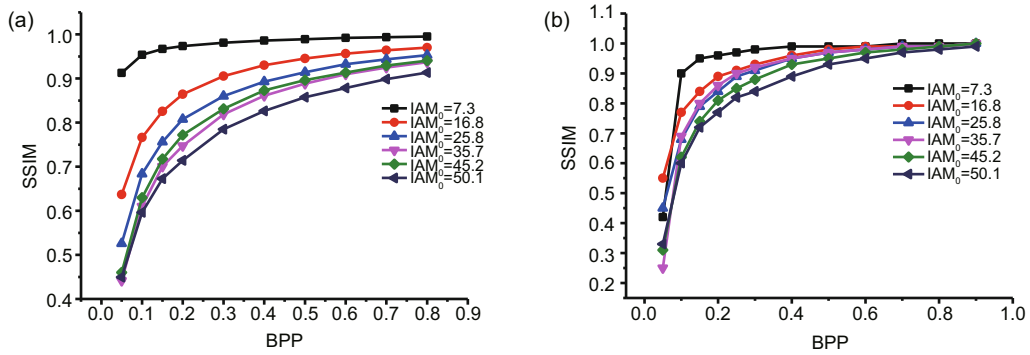

Fig. 7 BPP-SSIM curves of different image compressions: (a) SPIHT compression; (b) adaptive CS compression

SSIM: structural similarity; BPP: compression rate; IAM: image activity measurement; SPIHT: set partitioning in hierarchical trees; CS: compressive sensing

shape. The slope and position of each curve are the main differences, which are associated with the IAM_0 image value. The curves positioned in the upper left corner correspond to the images with low IAM_0 values, where the tilt slope of each curve is small, while curves in the lower right corner correspond to the images with large IAM_0 values, where the slope of the curve is larger.

In fact, the curve located in the upper left corner indicates that a low activity image can achieve higher compression quality when compared with a larger IAM image. When the compression rate of the image is lower than a certain threshold, the compression quality of the image sharply drops. This threshold is also related to image activity. In addition, the curve in the lower right area indicates that a larger IAM image needs a higher compression ratio to reach satisfactory image quality. The compression curves of a larger IAM image reach optimum quality with more stability.

According to the IAM_0 of the image, each BPP-SSIM curve has its own corresponding shape and slope, as the IAM_0 and BPP-SSIM curve are mapped in correspondence to each other. To verify this mapping relationship, nine images with similar IAM_0 values were selected (Fig. 8). Fig. 9 demonstrates their similar compression curves. Therefore, different quality curves can be distinguished by IAM_0, the shape and trend of the curve can be inferred according to IAM_0, and thus the compression quality curves of different images can be obtained.

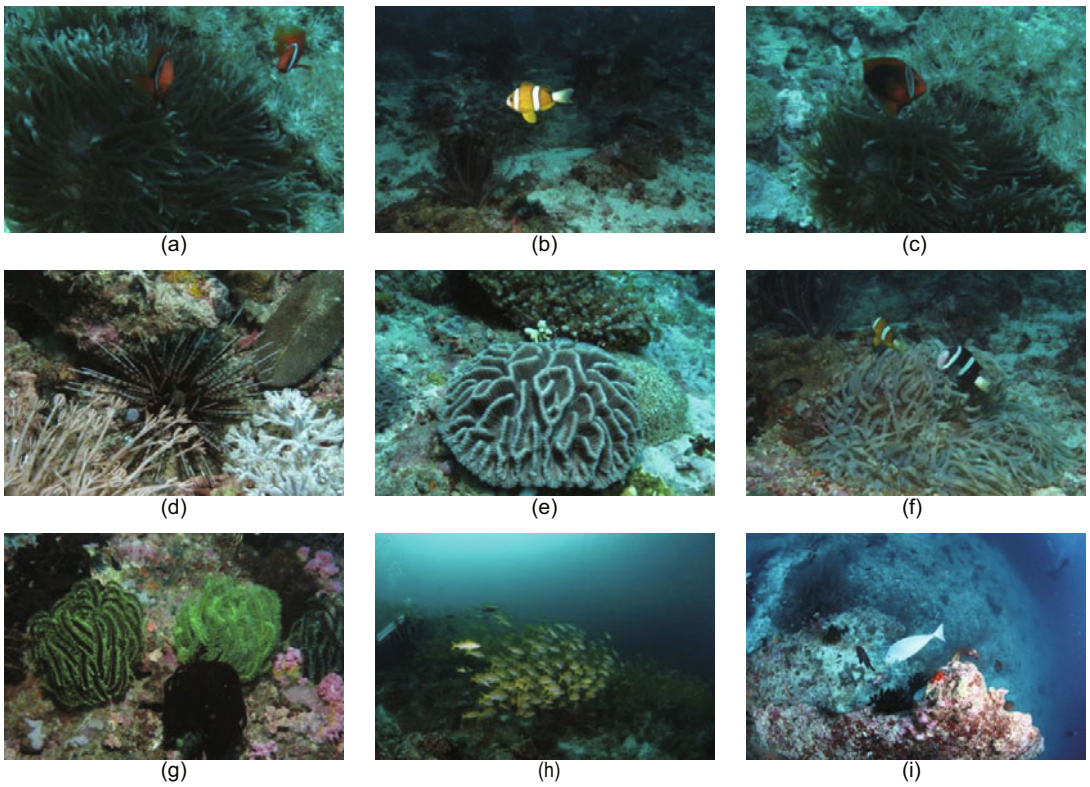

Fig. 8 Underwater images with similar IAM_0: (a) IMG11: IAM_0=30.3; (b) IMG2: IAM_0=35; (c) IMG12: IAM_0=35.6; (d) IMG6: IAM_0=35.7; (e) IMG13: IAM_0=37.1; (f) IMG1: IAM_0=41.3; (g) IMG17: IAM_0=41.6; (h) IMG4: IAM_0=41.9; (i) IMG7: IAM_0=45.2

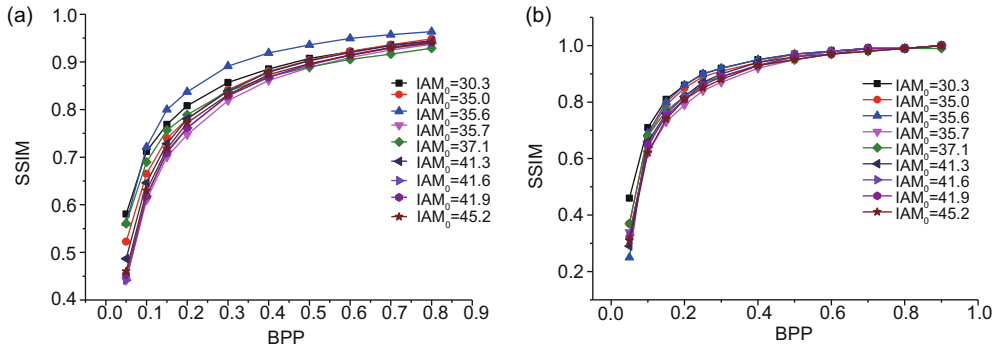

Fig. 9 BPP-SSIM curves of images with similar IAM_0: (a) SPIHT compression; (b) adaptive CS compression

SSIM: structural similarity; BPP: compression rate; IAM: image activity measurement; SPIHT: set partitioning in hierarchical trees; CS: compressive sensing

4 Fast quality estimation model for underwater image compression

4.1 Image quality estimation model

As demonstrated above in Section 3.3, the quality of a compressed image depends on the image compression ratio and IAM_0, and the image then follows the rules. The first rule is that the degree of curvature for each image compression quality curve is different. When the IAM_0 values of the images have a large difference, the curves have larger intervals, and when the IAM_0 values are similar, the interval between the curves is smaller. Each curve has its own specific curve slope. The second rule is that the rate of increase for the curve is different in different

BPP ranges. When BPP is below a certain threshold, SSIM rapidly increases with the increase of BPP, but when BPP is above a certain threshold, SSIM only slowly increases or tends to stabilize. In addition, the maximum objective quality that images can achieve is different; in other words, each image compression quality has its upper limit threshold.

According to the above image compression rules, the fitting function can be used to fit the BPP-SSIM curve. The perceived quality of service (PQoS) model (Koumaras et al., 2007) is that perceived quality can be described by a quality vector $\mathbf{QV} = (q_1, q_2, \ldots, q_n)$, where q is the parameter of influence for the quality vector. Therefore, the image compression quality can be expressed by the following parameters: parameter α determines the curve shape or slope, the compressed threshold $\mathrm{BPP_L}$, and the highest objective quality $\mathrm{SSIM_H}$ which the compressed image can achieve. In actual image compression, image compression quality needs to achieve a certain degree of human satisfaction, which means the image quality may demonstrate a certain distortion, but this distortion cannot affect the human eye's ability to obtain the important image information. Therefore, it is necessary to restrict the offline threshold $\mathrm{SSIM_L}$ for image quality. As a final point, the quality perception model for image compression is

$$\mathrm{SSIM} = (\mathrm{BPP_L}, \alpha, \mathrm{SSIM_H}, \mathrm{SSIM_L}). \tag{6}$$

To observe the curve of compression regularity in Figs. 7 and 9, the exponential function can be used as the fitting function, so the fitting function for the compressed quality of an underwater image can be set as

$$\mathrm{SSIM} = (\mathrm{SSIM_H} - \mathrm{SSIM_L})(1 - \mathrm{e}^{-\alpha(\mathrm{BPP}-\mathrm{BPP_L})}) + \mathrm{SSIM_L}. \tag{7}$$

When the SSIM value of the image is around 0.8, the image quality will be slightly blurred. Since the approximate texture information can be restored, however, the lowest acceptable compression quality can be taken as $\mathrm{SSIM_L} = 0.8$. Then, **QV** fitting is performed upon the underwater images in Fig. 6, and the corresponding fitting curves and fitting parameters are shown in Fig. 10 and Table 3, respectively.

Table 3 Quality vector fitting parameters in underwater image compression

Image	$\mathrm{IAM_0}$	α		$\mathrm{BPP_L}$		$\mathrm{SSIM_H}$	
		SPIHT	CS	SPIHT	CS	SPIHT	CS
IMG20	7.3	9.59	−0.05	0.99	35.74	0.08	0.99
IMG9	16.8	7.25	0.14	0.97	10.34	0.13	0.98
IMG19	25.8	6.59	0.20	0.95	9.09	0.16	0.98
IMG6	35.7	5.87	0.26	0.94	8.23	0.20	0.98
IMG7	45.2	6.34	0.24	0.94	9.43	0.19	0.97
IMG3	50.1	4.89	0.32	0.92	7.80	0.22	0.96

IAM: image activity measurement; SPIHT: set partitioning in hierarchical trees; CS: compressive sensing; α: curve shape or slope; $\mathrm{BPP_L}$: compressed threshold; $\mathrm{SSIM_H}$: highest objective quality

In Fig. 10, scatters are the actual quality of a compressed image, while curves are the fitting curves after exponential fitting; scatters and curve in the same color indicate correspondence with the same image. It can be seen from Fig. 10 that the SSIM value of each image can be fitted with a small error. The effectiveness of this fitting model is proven. After obtaining **QV** of the image compression quality,

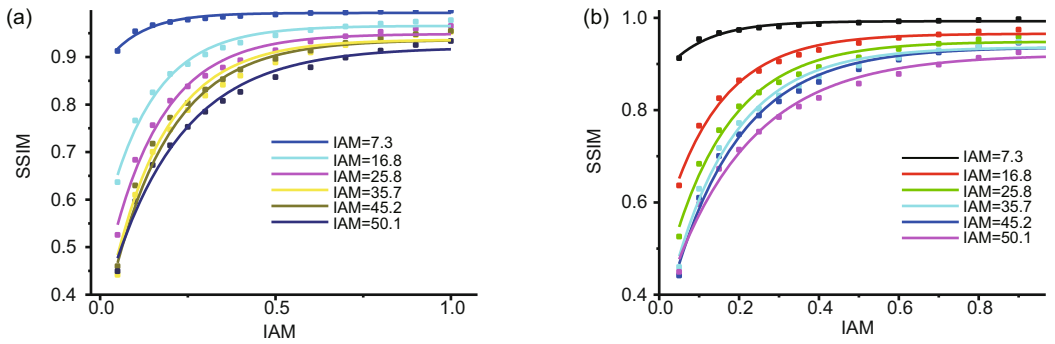

Fig. 10 Fitting curves for image compression quality: (a) SPIHT compression; (b) adaptive CS compression

References to color refer to the online version of this figure. SPIHT: set partitioning in hierarchical trees; CS: compressive sensing; SSIM: structural similarity; IAM: image activity measurement

image compression quality under any compression ratio can be attained according to the fitting formula. Fig. 11 shows the process diagram. First the IAM_0 values of the input image and the corresponding **QV** are calculated, then the compression quality estimation formula of the corresponding image is obtained, and finally BPP is plugged into the formula to estimate compression quality.

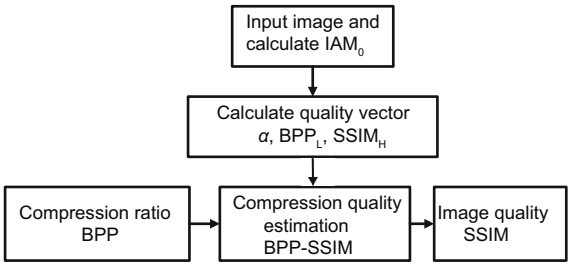

Fig. 11 Image compression quality estimation process

4.2 Quality vector in fast estimation

When there is a one-to-one correspondence between **QV** and an image, compression quality can be concluded after obtaining **QV**. However, as multiple **QV** are difficult to obtain, a multitude of fitting calculations needs to be performed. 100 images are selected to calculate **QV**, from which the scatters between the fitting parameters and IAM can be obtained. Several images are selected in each IAM_0 range, and the scatters are shown in Fig. 12. Such one-to-one correspondence between **QV** and IAM_0 is demonstrated in Fig. 12, where in fact the quality curve of each image is associated with IAM. Quality curves with smaller IAM_0 values tend to stabilize faster and show a smaller slope. If the highest compression quality is larger, the compression ratio will be smaller under the same quality curve. Thus, fitting parameters can be estimated based on the IAM_0 of an image, from which the compression quality curve can be obtained.

As established by Fig. 12, it can be observed that the relevant parameters have a linear relationship, so the parameters are fitted in the form of

$$y=\sum_{k=0}^{n} b_k x_k = b_0 + b_1 x + b_2 x^2 + \ldots + b_n x^n, \quad (8)$$

where b_k is a constant.

The first two items are picked to fit $SSIM_H$ and BPP_L, and the first three items are picked to fit α. The fitting scatter diagrams of SPIHT and adaptive CS compressions are shown in Fig. 13, and the fitting results are

$$\begin{cases} \mathrm{SSIM_{H\text{-}SPIHT}} = 0.9913 - 0.0013\mathrm{IAM_0}, \\ \alpha_{\mathrm{SPIHT}}=9.503–0.1190\mathrm{IAM_0}+0.0008\mathrm{IAM_0^2}, \\ \mathrm{BPP_{L\text{-}SPIHT}} = 0.0283 + 0.0054\mathrm{IAM_0}, \end{cases} \quad (9)$$

$$\begin{cases} \mathrm{SSIM_{H\text{-}CS}} = 0.9949 + 0.00157\mathrm{IAM_0}, \\ \alpha_{\mathrm{CS}}=4.8045-0.0731\mathrm{IAM_0}+0.0004\mathrm{IAM_0^2}, \\ \mathrm{BPP_{L\text{-}CS}} = 0.0117 + 0.0157\mathrm{IAM_0}. \end{cases} \quad (10)$$

There are some differences in the fitting effect of the parameters, but the final estimation error is within the allowable range. Through fast estimation of **QV**, the IAM_0 value can be calculated after image input, and a set of quality vector parameters obtained according to the linear relationship among **QV** and IAM. Thus, the image compression quality BPP-SSIM curve is obtained. The whole process does not require image encoding, since when the compression ratio is known, image compression quality can be estimated by direct mapping.

4.3 Image compression with fixed perception quality value

In the image compression process, the compression ratio is generally set based on the channel conditions. However, this leads to an inability to predict image quality, which may produce the problem where image quality cannot meet the demands of human visual perception after coding compression and transmission. Instead, if the image compression ratio is set according to the perception quality, the above situation can be avoided and each image is effectively compressed with high quality. Therefore, the above compression estimation formula will be able to solve the problem after inverse mapping is done.

After obtaining the specific relationship between image quality and compression ratio, image quality can be estimated through the compression ratio. Inversely, the image compression rate can be calculated according to the required quality of the compressed image in the transmission system. According to Eq. (6), the relationship between BPP and SSIM can be obtained as

$$\mathrm{BPP} = \mathrm{BPP_L} - \frac{\ln\left(1-\frac{\mathrm{SSIM}-\mathrm{SSIM_L}}{\mathrm{SSIM_H}-\mathrm{SSIM_L}}\right)}{\alpha}, \quad (11)$$

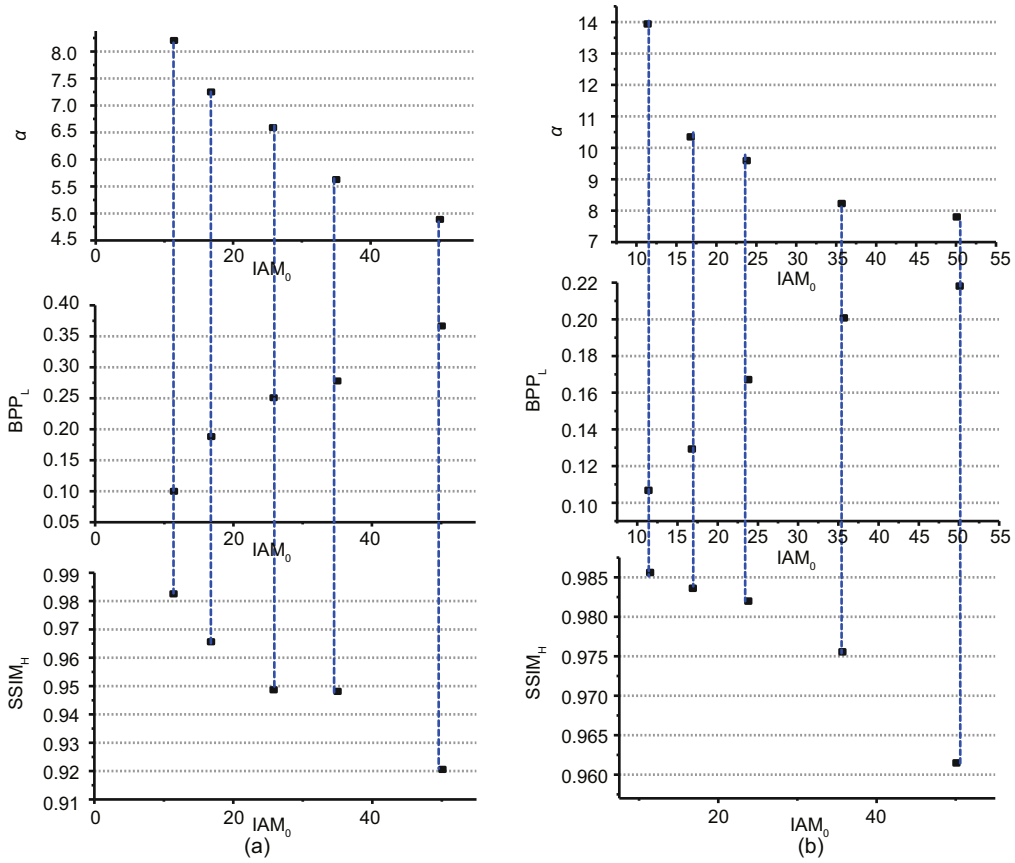

Fig. 12 Scatter diagrams of compression quality fitting parameters: (a) SPIHT compression fitting; (b) adaptive CS compression fitting

IAM: image activity measurement; SPIHT: set partitioning in hierarchical trees; CS: compressive sensing; α: curve shape or slope; BPP_L: compressed threshold; $SSIM_H$: highest objective quality

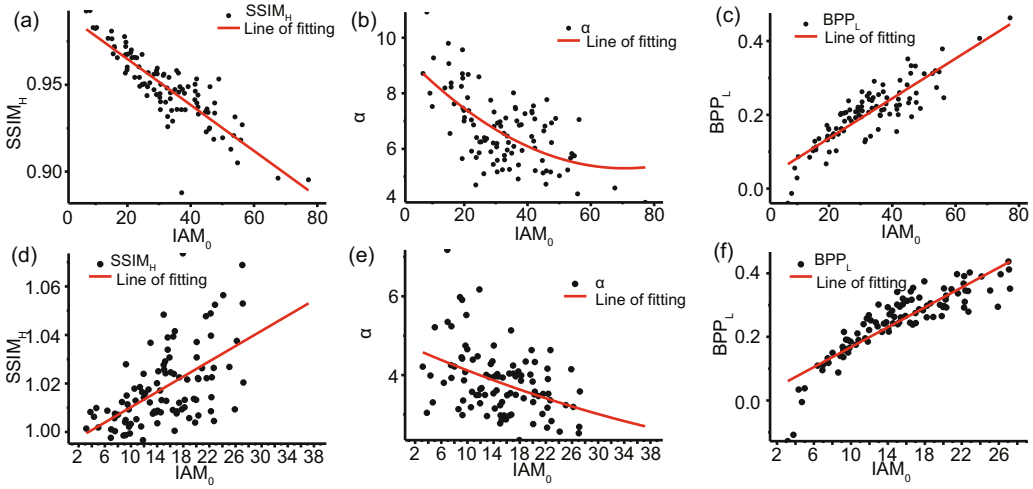

Fig. 13 Quality fitting parameter scatter and fitting curves: (a) $SSIM_H$ of SPIHT compression; (b) α of SPIHT compression; (c) BPP_L of SPIHT compression; (d) $SSIM_H$ of adaptive CS compression; (e) α of adaptive CS compression; (f) BPP_L of adaptive CS compression

IAM: image activity measurement; SPIHT: set partitioning in hierarchical trees; CS: compressive sensing; α: curve shape or slope; BPP_L: compressed threshold; $SSIM_H$: highest objective quality

where $\mathrm{BPP_L}$, $\mathrm{SSIM_H}$, and α can be obtained according to the linear relation in Eqs. (9) and (10).

To meet an accurate application of compressed image quality, a linear interpolation method was proposed in Zemliachenko et al. (2016). The accuracy of the estimation formula is further improved by no more than two image coding and decoding calculation processes. The process diagram is as shown in Fig. 14. BPP_1 and its corresponding actual perception quality Q_1 are firstly calculated. If Q_1 and the desired compression quality Q are within an acceptable precision error range, there is no need for a second calculation, and the final compression ratio $\mathrm{BPP}_0 = \mathrm{BPP}_1$. If Q_1 is greater than the permissible error range, an interpolation calculation is performed. When $Q_1 > Q$, the second compression ratio is set as $\mathrm{BPP}_2 = \mathrm{BPP}_1 - \Delta\mathrm{BPP}$, and when $Q_1 < Q$, the second compression ratio is set as $\mathrm{BPP}_2 = \mathrm{BPP}_1 + \Delta\mathrm{BPP}$, where $\Delta\mathrm{BPP}$ is a small step compression ratio for interpolation. Then the actual quality Q_2 of the image compressed by the interpolation compression ratio can be calculated. The final precise compression rate after interpolation is

$$\mathrm{BPP}_0 = \frac{Q - Q_1}{Q_2 - Q_1}(\mathrm{BPP}_2 - \mathrm{BPP}_1) + \mathrm{BPP}_1. \quad (12)$$

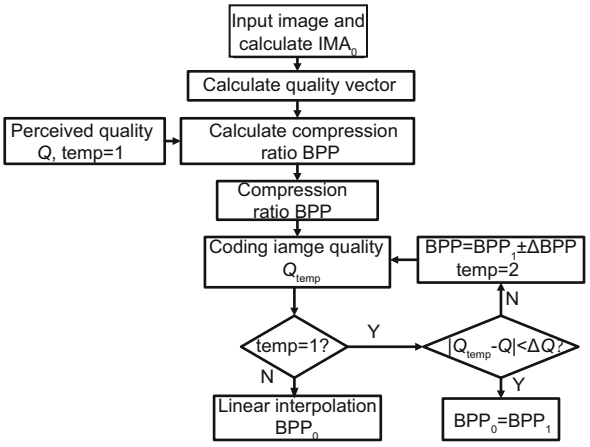

Fig. 14 Linear interpolation flowchart for fixed value compression

5 Experiments

5.1 Verification of the quality estimation model

To analyze the performance of the quality estimation formula, 110 underwater optical images were selected for estimation analysis. First, the IAM_0 of the image was calculated according to Eqs. (9) and (10) respectively, and SPIHT compression and CS compression curve parameters were calculated respectively. Then the obtained parameters were plugged into Eq. (7) to obtain the image compression quality fitting function. The compression quality value was predicted by substituting the independent variable BPP into the fitting function. The comparison of the estimation curve with the actual compression curve of three images (Fig. 15) is shown in Fig. 16, where the black curve is the actual compression curve and the red curve is the predicted curve. It can be seen from Fig. 16 that the quality value obtained by compression estimation is similar to the actual compression value. The error distribution between the estimated value and the actual value of the 110 images at BPP from 0.05 to 1.0 is summarized in Fig. 17.

In Fig. 16, the difference between the image estimation quality curve and the actual compression curve is small, which abundantly demonstrates the effectiveness of the estimation model and the estimation parameters. As shown in Fig. 17, when the compression ratio is greater than 0.2, the error between the predicted value of the image compression quality and the actual value does not exceed 0.05. When the

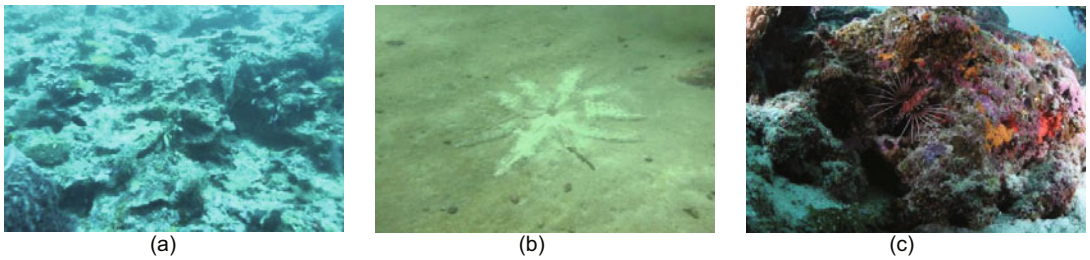

Fig. 15 Underwater images for testing: (a) IMG112: $\mathrm{IAM_0}$=37.46; (b) IMG141: $\mathrm{IAM_0}$=12.45; (c) IMG180: $\mathrm{IAM_0}$=53.07

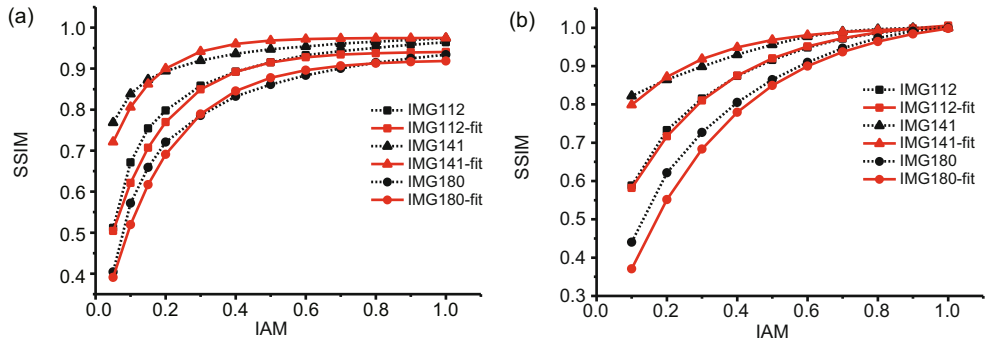

Fig. 16 Comparison curves between the actual value and predicted value of compression quality: (a) SPIHT compression prediction; (b) adaptive CS compression prediction

The black curve is the actual compression quality and the red curve is the fitting quality. References to color refer to the online version of this figure. SPIHT: set partitioning in hierarchical trees; CS: compressive sensing

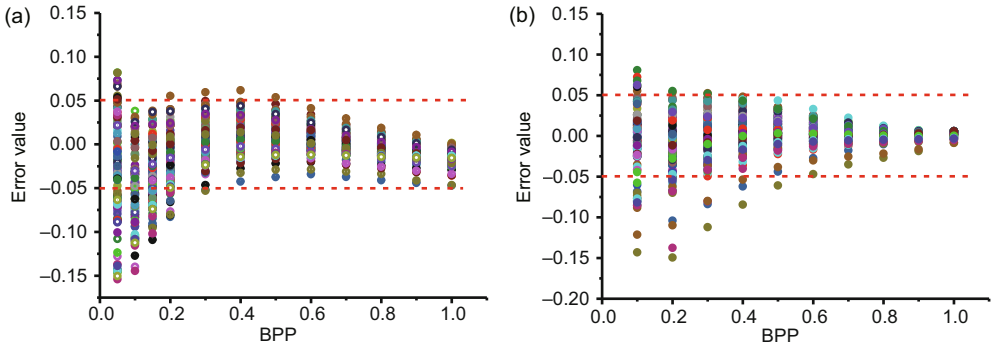

Fig. 17 Error statistics between the predicted value and actual value of image compression: (a) set partitioning in hierarchical trees (SPIHT) compression error; (b) adaptive compressive sensing (CS) compression error

compression ratio is less than 0.2, the compression quality error of the image is within the range of −0.15 to 0.1. However, when BPP $<$ 0.2, and most of the image compression quality is SSIM $<$ 0.8, the image reconstruction effect is poor. Therefore, this quality range of the reconstructed image is generally not used. Thus, the quality estimation of a compressed image in this BPP range does not affect the estimation model when used in actual image transmission, so accuracy and practicality can be assumed.

5.2 Experiment on compression quality with fixed value

Assume that in the channel transmission process, the requirement is to obtain a compressed image where the SSIM quality is equal to 0.90. This necessitates setting the required quality value as 0.9, selecting three different images randomly, obtaining the corresponding compression ratio BPP according to Eq. (11), and then calculating the precise compression ratio by the interpolation method to verify the actual compression quality under this doubled compression ratio. In the interpolation method, to obtain more accurate compression quality, the error threshold is set at $\Delta Q = 0.0125$ and the compression rate step is set at $\Delta\text{BPP} = 0.1$. The list of parameters obtained by verification is shown in Table 4, and the SPIHT compressed image obtained before and after interpolation is shown in Fig. 18. As can be seen from Table 4, the compression ratio is obtained under the condition of fixed image quality. The difference between the actual compression quality and the specified quality is within the acceptable range, as all are below 0.05. Image quality can be obtained even more accurately with the linear interpolation method; in other words, the compression image quality has higher accuracy. When the image quality corresponding to a compression rate calculated directly is larger than the assigned quality, namely $\text{SSIM}_1 > \text{SSIM}$, the compression ratio is reduced by the interpolation calculation. In the

Table 4 Compression ratio and actual quality with fixed image quality

Type	Image	IAM_0	BPP_L	α	$SSIM_H$	Direct calculation		Interpolation calculation	
						BPP_1	$SSIM_1$	BPP_0	$SSIM_0$
SPIHT	IMG119	21.455	0.144	7.338	0.963	0.274	0.860	0.394	0.898
	IMG147	32.167	0.202	6.547	0.949	0.373	0.936	0.211	0.889
	IMG156	63.000	0.369	5.349	0.908	0.853	0.938	0.548	0.891
CS	IMG119	21.455	0.174	4.093	1.011	0.331	0.929	0.266	0.903
	IMG147	32.167	0.216	3.922	1.015	0.222	0.920	0.204	0.910
	IMG156	63.000	0.478	3.018	1.041	0.445	0.938	0.353	0.902

IAM: image activity measurement; SPIHT: set partitioning in hierarchical trees; CS: compressive sensing; α: curve shape or slope; BPP_L: compressed threshold; $SSIM_H$: highest objective quality; BPP: compression rate; SSIM: structural similarity

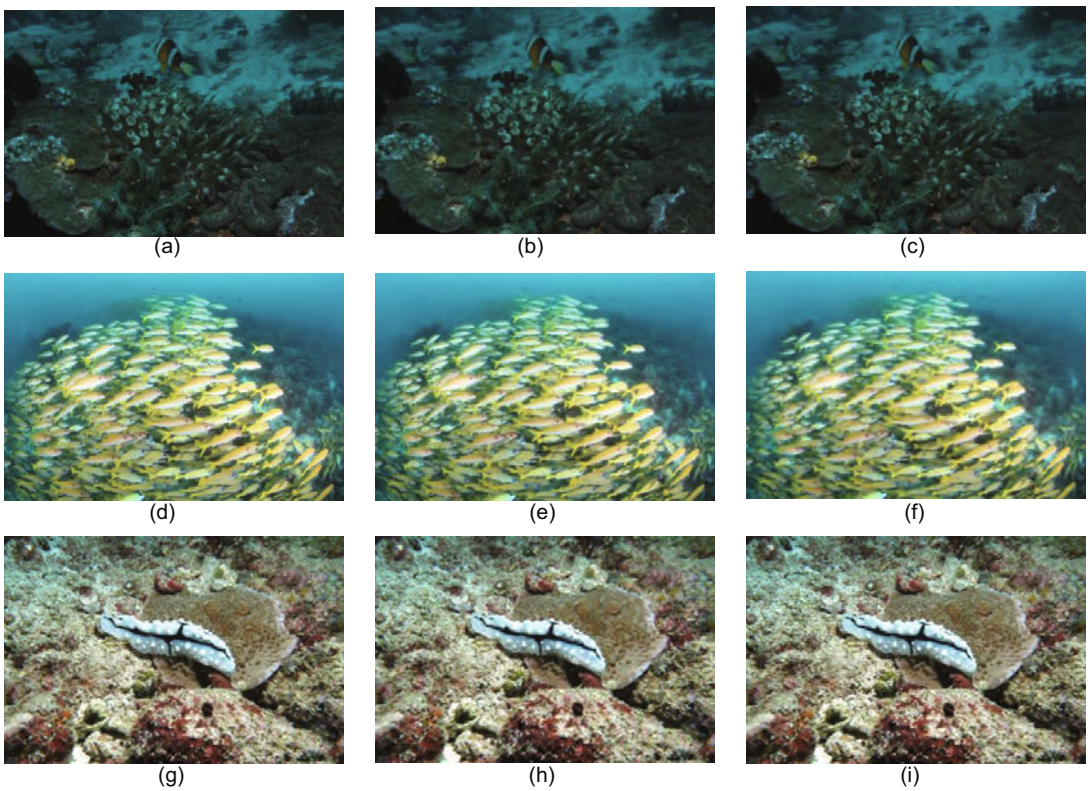

Fig. 18 Image compression quality comparison before and after interpolation: (a) reference image IMG119: IAM_0=21.45; (b) before interpolation: BPP=0.27, SSIM=0.86; (c) after interpolation: BPP=0.39, SSIM=0.89; (d) reference image IMG147: IAM_0=32.17; (e) before interpolation: BPP=0.39, SSIM=0.94; (f) after interpolation: BPP=0.21, SSIM=0.89; (g) reference image IMG156: IAM_0=63.0; (h) before interpolation: BPP=0.85, SSIM=0.94; (i) after interpolation: BPP=0.55, SSIM=0.89

IAM: image activity measurement; BPP: compression rate; SSIM: structural similarity

SPIHT compression of IMG156, Fig. 18h is the image obtained by direct calculation with a compression ratio of 0.8529, and Fig. 18i is the image obtained by interpolation calculation with a compression ratio of 0.5480. The quality of the two images is not visually different, but the compression rate after interpolation is greatly reduced, so the data transmitted in the system will also be greatly reduced. Therefore, this complexly textured image can have its compression rate reduced by calculating the compression ratio with the interpolation method, which effectively improves the efficiency of the image communication system while not affecting image quality. When $SSIM_1$<SSIM, interpolation calculation can

improve both compression rate and image quality, so that the quality of the reconstructed image is within the required accuracy range.

6 Conclusions

IAM can measure the textural complexity of an image and have a close relationship with the image compression quality. This study first discussed the rules of compression quality of underwater images in conjunction with different compression methods, and the distorted characteristics of image compression were summarized. Then the quality vector was used to analyze and evaluate image quality to demonstrate that by using the image quality prediction formula, the corresponding image quality could be calculated without image encoding. Therefore, on the one hand, the method can guarantee the quality of a compressed image; on the other hand, the prediction results can be used to guide the encoding strategy choice and to determine coding parameters. In addition, using the inverse function prediction formula, the relationship between the image compression ratio and compression quality can be obtained, and the linear interpolation improvement scheme can be used to further improve the accuracy of image compression quality.

References

Atallah AM, Ali HS, Abdallsh MI, 2016. An integrated system for underwater wireless image transmission. 28th Int Conf on Microelectronics, p.169-172. https://doi.org/10.1109/ICM.2016.7847936

Candès EJ, Romberg J, Tao T, 2006. Robust uncertainty principles: exact signal reconstruction from highly incomplete frequency information. *IEEE Trans Inform Theory*, 52(2):489-509. https://doi.org/10.1109/TIT.2005.862083

Chen WL, Yuan F, Cheng E, 2016. Adaptive underwater image compression with high robust based on compressed sensing. IEEE Int Conf on Signal Processing, p.1-6. https://doi.org/10.1109/ICSPCC.2016.7753722

Donoho DL, 2006. Compressed sensing. *IEEE Trans Infrom Theory*, 52(4):1289-1306. https://doi.org/10.1109/tit.2006.871582

Koumaras H, Kourtis A, Martakos D, et al., 2007. Quantified PQoS assessment based on fast estimation of the spatial and temporal activity level. *Multim Tools Appl*, 34(3):355-374. https://doi.org/10.1007/s11042-007-0111-1

Kourzi A, Nuzillard D, Millon G, et al., 2005. Quality estimation in wavelet image coding. Proc 13th European Signal Processing Conf, p.1-4.

Liu A, Lin W, Narwaria M, 2012. Image quality assessment based on gradient similarity. *IEEE Trans Image Process*, 21(4):1500-1512. https://doi.org/10.1109/TIP.2011.2175935

Ponomarenko N, Silvestri F, Egiazarian K, et al., 2007. On between-coefficient contrast masking of DCT basis functions. 3rd Int Workshop on Video Processing and Quality Metrics, p.1-4.

Saha S, Vemuri R, 2002. An analysis on the effect of image features on lossy coding performance. *IEEE Signal Process Lett*, 7(5):104-107. https://doi.org/10.1109/97.841153

Said A, Pearlman WA, 1996. A new fast and efficient image codec based on set partitioning in hierarchical trees. *IEEE Trans Circu Syst Video Technol*, 6(3):243-250. https://doi.org/10.1109/76.499834

Sarita K, Meel VS, Ritu V, 2011. Image quality prediction by minimum entropy calculation for various filter banks. *Int J Comput Appl*, 7(5):31-34. https://doi.org/10.5120/1158-1434

Sheikh HR, Bovik AC, 2006. Image information and visual quality. *IEEE Trans Image Process*, 15(2):430-444. https://doi.org/10.1109/TIP.2005.859378

Sophia PE, Anitha J, 2016. Region-Based Prediction and Quality Measurements for Medical Image Compression. Springer, Singapore. https://doi.org/10.1007/978-981-10-0448-3_29

Tang CQ, Tian GY, Li KJ, et al., 2017. Smart compressed sensing for online evaluation of CFRP structure integrity. *IEEE Trans Ind Electron*, 64(12):9608-9617. https://doi.org/10.1109/TIE.2017.2698406

Tichonov J, Kurasova O, Filatovas E, 2016. Quality prediction of compressed images via classification. 8th Int Conf on Image Processing and Communications Challenges, p.35-42. https://doi.org/10.1007/978-3-319-47274-4_4

Wang Z, Bovik AC, 2002. A universal image quality index. *IEEE Signal Process Lett*, 9(3):81-84. https://doi.org/10.1109/97.995823

Wang Z, Simoncelli EP, Bovik AC, 2003. Multiscale structural similarity for image quality assessment. 37th Asilomar Conf on Signals, Systems and Computers, p.1398-1402. https://doi.org/10.1109/ACSSC.2003.1292216

Wang Z, Bovik AC, Sheikh H, et al., 2004. Image quality assessment: from error visibility to structural similarity. *IEEE Trans Image Process*, 13(4):600-612. https://doi.org/10.1109/TIP.2003.819861

Xue WF, Zhang L, Mou XQ, et al., 2014. Gradient magnitude similarity deviation: a highly efficient perceptual image quality index. *IEEE Trans Image Process*, 23(2):684-695. https://doi.org/10.1109/TIP.2013.2293423

Zemliachenko A, Lukin V, Ponomarenko N, et al., 2016. Still image/video frame lossy compression providing a desired visual quality. *Multidimens Syst Signal Process*, 27(3):697-718. https://doi.org/10.1007/s11045-015-0333-8

Zhang L, Zhang L, Mou X, et al., 2011. FSIM: a feature similarity index for image quality assessment. *IEEE Trans Image Process*, 20(8):2378. https://doi.org/10.1109/TIP.2011.2109730